RSC Advances

ROYAL SOCIETY OF CHEMISTRY

www.rsc.org/advances

Cite this: DOI: 10.1039/c0xx00000x

www.rsc.org/xxxxxx

ARTICLE TYPE

Preferential interaction of small-diameter metallic SWNTs with ferroelectric polymer

Mengmeng Ye, Zhi-Jun Qiu,* Hui Li, Minni Qu and Ran Liu*

Received (in XXX, XXX) Xth XXXXXXXXX 20XX, Accepted Xth XXXXXXXXX 20XX

DOI: 10.1039/b000000x

Poly(vinylidene difluoride) (PVDF) blends with single-walled carbon nanotubes (SWNTs) have been prepared to investigate the interaction between nanotubes and polymer. The SWNTs are observed to form a well-dispersion in the fluoropolymer matrix. Raman measurements showed sizable changes in the frequencies and intensities of SWNTs and PVDF in the composites compared with the values in pristine SWNTs and neat PVDF. This originates from the polymer's preferably interacting with metallic SWNTs (m-SWNTs), especially with small-diameter tubes due to non-vanishing Fermi electrons and increased curvature-induced strain energy. In addition, the selective dispersion of m-SWNTs induced remarkable enhancement in the β ferroelectric phase of PVDF as demonstrated in Fourier transform infrared spectroscopy (FTIR).

Introduction

Poly(vinylidene fluoride) (PVDF) is an important semicrystalline thermoplastic, and has been extensively studied because of its potential applications as piezoelectric, pyroelectric, or electrocaloric materials, which can be used in supercapacitors, actuators, batteries, nonlinear optical fields, and cooling technologies.[1-6] It has five different crystalline forms (α, β, γ, δ, ε), in which the nonpolar α- and polar β-phases are the main crystalline polymorphs.[7,8] The α-phase has alternation trans- and gauche-bond conformation and is the most common and stable polymorph. The β-phase has an all-trans conformation comprising fluorine atoms and hydrogen atoms on opposite sides of the polymer backbone, which results in the non-zero dipole moment, and thus exhibits outstanding piezoelectric, pyroelectric, and ferroelectric properties.

A variety of experimental techniques have been developed to induce desirable β-phase formation. The polar β-phase in PVDF is generally obtained by uniaxial or biaxial drawing of α-phase films,[9] poling in a strong electric field,[10] ultra-fast quenching,[11] and crystallization under high pressure.[12] Recently, the incorporation of nanofillers has been in focus as means of enhancing the formation of β-phase in PVDF.[7,13-16] Among the various nanofillers used in PVDF nanocomposites, carbon nanotubes (CNTs) have been considered as ideal reinforcing fillers due to a combination of remarkable electrical, thermal and mechanical properties. Polymer/CNT nanocomposites have been demonstrated with higher stiffness, higher modulus, improved dimensional stability, decreased coefficient of thermal expansion and better electrical conductivity at relatively low CNT concentration.[17,18] Due to the zigzag carbon atoms on the CNT surface, which match with the all-trans conformation of β-phase PVDF, the crystallization of PVDF in the β-polymorphic structure is induced resultantly. Also, the high aspect ratio of CNTs leads to a very low percolation threshold in the polymer nanocomposite.

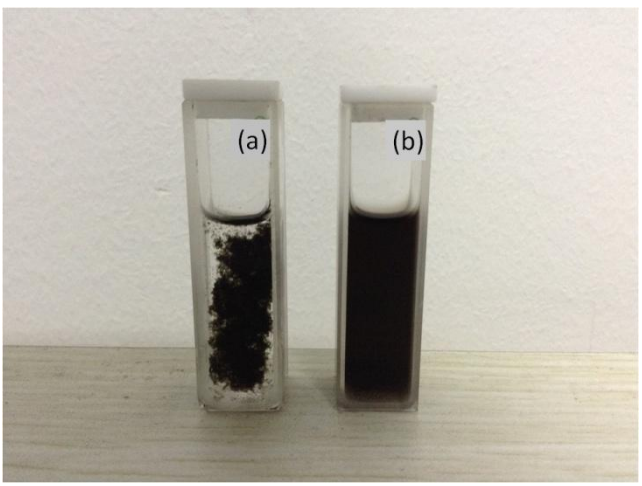

Fig. 1 Photographs of SWNTs dispersed in N,N-dimethylformamide (DMF) solvent (a) and SWNTs dispersed in PVDF-DMF solution (b).

Although much work on nanocomposites composed of PVDF and multi-walled CNTs (MWNTs) have been reported,[19-21] the investigation on the single-walled CNTs (SWNTs) as conductive nanofillers is relatively scarce, especially on the interaction mechanism between SWNTs and PVDF,[22] to our knowledge. In our work, the dependence of nanotube metallicity on the interface interaction between SWNTs and PVDF has been investigated and found that the metallic SWNTs (m-SWNTs) with small diameters are favorable to bond with PVDF polymer, resulting in enhanced ferroelectric β phase of PVDF.

Results and discussion

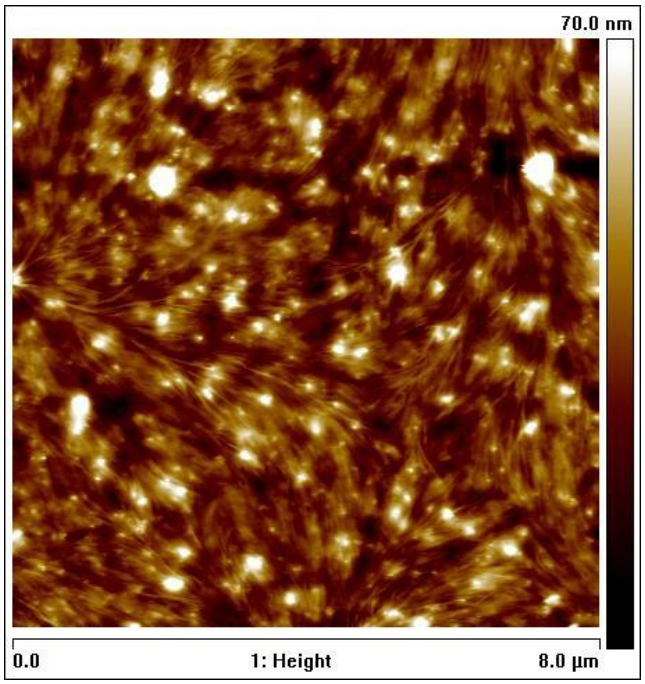

Fig. 2 AFM images of SWNTs dispersed in the PVDF host.

As shown in Fig. 1, in contrast to rapid precipitation of SWNTs dispersed in DMF solvent, no settling or segregation of SWNTs in PVDF/DMF solution was observed, even after storing for several months, indicating good dispersion of SWNTs in PVDF/DMF solution. It is worth noting that the homogeneous solution cannot be obtained by adding PVDF solution drop wise to SWNT suspensions. In this case, an excess of SWNTs will exist relative to the polymer, leading to a risk of forming flocculation. Conversely, if the SWNT suspension is added to the polymer solution, the polymer is in excess during the process. As a result, the polymer chain could adsorb onto the SWNT surface, leading to stable dispersion.

The atomic force microscopy (AFM) image of the composite film in Fig. 2 clearly indicates individual SWNTs being sparsely embedded in the polymer host. The random-dispersed bright lines are SWNTs, and bright dots are the ends of the broken SWNTs.[23] Yuan et al. suggested that a donor-acceptor interaction occurring between delocalized π electrons of CNTs and strongly electrophilic F groups of PVDF chain promotes a homogeneous dispersion of the CNTs in PVDF matrix through non-covalent bonding.[24]

Raman spectroscopy with 514-nm excitation wavelength is used to examine the interaction between the SWNTs and the polymer. Fig. 3a shows the low-frequency radial breathing modes (RBM) of the pristine SWNTs and the SWNTs in the composite. The collected spectra are separated and offset vertically for clarity after normalization to the most intensified peak. In Fig. 3a, we clearly observed two groups of semiconducting SWNTs (s-SWNTs) near 200 cm^{-1} and m-SWNTs near 260 cm^{-1} in the RBM spectra. The characteristics of s- and m-SWNTs were determined from the Kataura plot that is expressed by the relationship between transition energies and nanotube diameter.[25] When the energy of the incident laser matches the allowed electronic transitions between van Hove singularities of a particular nanotube, Raman signals of the nanotube are resonantly enhanced.

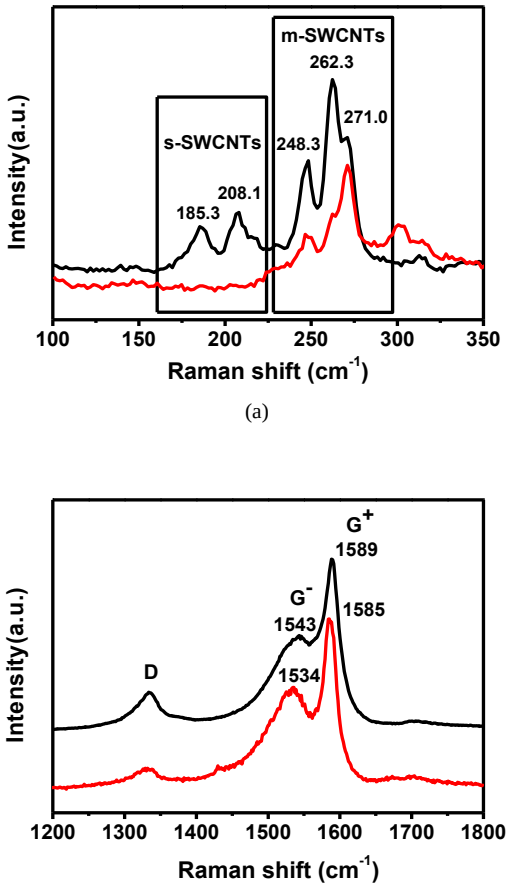

Fig. 3 Raman spectra of RBM (a) and G band (b) in pristine SWNTs (black) and PVDF composite (red).

Table I Fraction of m-SWNTs with different diameters in pristine SWNTs and composite.

RBM(cm^{-1})/d(nm)	271/0.86	262.3/0.90	248.3/0.95
Pristine SWNTs	29.3%	46.8%	23.9%
PVDF/SWNT composite	58.4%	24.3%	17.3%

At 514 nm, the excitation is resonant with the E_{33}^{S} transition in s-SWNTs and the E_{11}^{M} transition in m-SWNTs. It is found that the two prominent RBM peaks at 185.3 and 208.1 cm^{-1} from s-SWNTs disappear in the composite, while those peaks at 248.3, 262.3 and 271 cm^{-1} from m-SWNTs still exist. Interestingly, the relative intensity of the peak at 271 cm^{-1} becomes large. The diameters (d) of SWNTs were determined by the following relation with Raman shifts (ω_{RBM}):[26]

$$\omega_{\mathrm{RBM}}(\mathrm{cm}^{-1}) = \frac{223.5}{d(\mathrm{nm})} + 12.5 \quad (1)$$

The fraction of m-SWNTs with various diameters is calculated using the ratio of the peak areas, which is obtained through a Lorentzian fit of the RBM peaks. As shown in table I, the fraction of small-diameter (0.86 nm) m-SWNTs in composite is increased

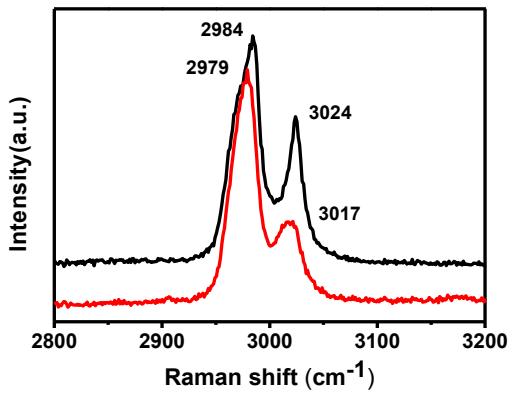

Fig. 4 Raman spectra of C-H vibrations in neat PVDF (black) and its composite (red).

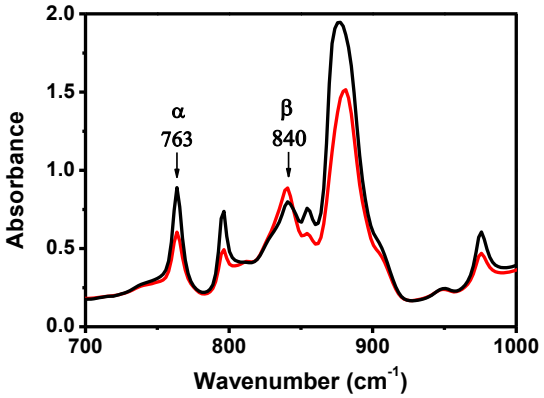

Fig. 5 FTIR spectra of neat PVDF (black) and its composite (red).

two-fold compared to that in the pristine SWNTs. The lack of RBM signals from s-SWNTs in the composite was probably caused by the selective removing of s-SWNTs bundles in the centrifugation process, due to stronger van der Waals interaction among the s-SWNTs than s-SWNT-polymer interaction. In contrast, more available charge density at the Fermi level promotes charge transfer from m-SWNTs to PVDF polymer.

Furthermore, the distinct selectivity preferring the small-diameter m-SWNTs can be understood under the mechanism of curvature-induced strain energy in the interaction between PVDF and m-SWNTs. The curvature-induced strain energy in a nanotube per carbon atom, including contributions of pyramidalization angle and π-orbital misalignment, has been shown to be inversely related to nanotube diameter.[27] The higher strain energy in smaller diameter tubes renders them more reactive than larger diameter tubes, which is responsible for the diameter dependence of interface reaction between nanotubes and PVDF. Similar changes in the RBM frequencies have been observed when SWNTs are functionalized with other polymers.[28,29]

The strong metallicity-dependent dispersion in PVDF/SWNT composite was further demonstrated in the Raman spectra of the tangential mode (G band). As shown in Fig. 3b, an intensified and 9-cm^{-1} downshift of Breit–Wigner–Fano (BWF) line shape (G^- peak) around 1540 cm^{-1} and the 4-cm^{-1} downshift of G^+ peak around 1590 cm^{-1}, are observed in the composite compared to the pristine SWNTs. For SWNTs, the G band typically is composed of two separate peaks, G^+ and G^-. The strong phonon-plasmon coupling in the m-SWNTs results in downshift and asymmetric BWF line shape for G^- peak relative to s-SWNTs.[30] Besides it, the TO-dominant G^+ of metallic tubes is lower than LO-dominant G^+ of s-SWNTs due to zone folding effect.[31] It is also noticed that, accompanied by the shift of G band, the intensity of disorder-induced mode (D band) at 1350 cm^{-1} in the composite is also greatly reduced as compared with the pristine sample, leading to increase of G/D ratio. This behavior seems counterintuitive to other polymer-functionalized SWNTs, where D-band intensity should be enhanced in that chemical functionalization disrupted the structure of the SWNTs and introduced more defects in the nanotubes. Our results may be attributed to the centrifugal sedimentation, which removes undispersed amorphous carbon, graphitic particles, and other carbon nanoparticles in the composite.

The molecular-level interaction between SWNTs and PVDF matrix can be further confirmed by the change of Raman spectra in PVDF, as shown in Fig. 4. The C-H stretch modes around 3000 cm^{-1} are the only modes of the polymer observed in the Raman spectra. In order to insure that the treatment in the composite preparation did not produce changes observed, the polymer without SWNTs was subjected to the same sonication, centrifugation and heat treatment as the composite. It was found that the C-H stretch modes were shifted from 2984 and 3024 cm^{-1} in pristine PVDF to 2979 and 3017 cm^{-1} in composite, and also, the peak at 2979 cm^{-1} is intensified relative to the higher frequency. These effects again indicate a bonding of the polymer to the SWNTs, especially m-SWNTs with small diameter.

Though the crystal lattice energy of β-phase is slightly lower than that of the α-phase, direct β-phase formation from the solution is prohibited in the PVDF due to the high energy barriers required for transforming alternation trans- and gauche-bond conformation into all-trans conformation.[32] It was reported that ultrasonic cavitation occurred in the sonication process can generate a local temperature as high as 5000 K, local pressure as high as 50.6 MPa, and heating / cooling rate greater than 10^9 K/s.[33] Under such conditions, PVDF chains are subjected to extremely large forces near collapsing cavitation bubbles. In this process, α-phase polymer chains will obtain energy from the sonicating solution, which can easily overcome the energy barrier to be converted to β-phase. The transformed β-phase molecular chain prefers to be absorbed on the surface of m-SWNTs and act as nucleating agents for the crystallization of polymer chains. The formation of β phase was confirmed by the absorption peaks in the Fourier transform infrared (FTIR) spectra in Fig. 5. In the previous reports, the vibration band at 763 cm^{-1} is assigned to CF_2 bending and skeletal bending of α-phase, whereas the 840 cm^{-1} band is ascribed to a mixed mode of CH_2 rocking and CF_2 asymmetric stretching vibration in β-phase PVDF. The fraction of β-phase, $F(\beta)$, can be calculated using the following equation:[34]

$$F(\beta) = \frac{A_\beta}{1.26A_\alpha + A_\beta} \quad (2)$$

where A_α and A_β are the absorbances of α- and β-phase at 763 and 840 cm^{-1}, respectively. As indicated, the fraction of β-phase is increased from 19% to 32%, suggesting that the preferable

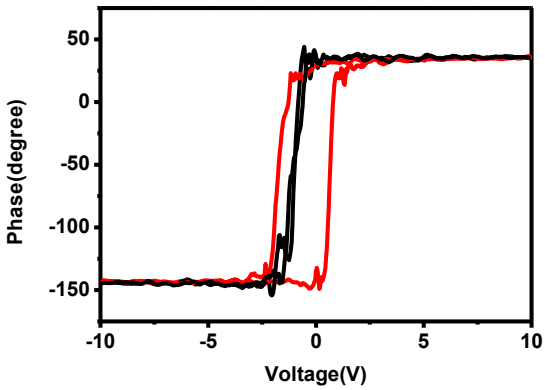

Fig. 6 ferroelectric hysteresis loops of neat PVDF (black) and its composite (red).

dispersion of m-SWNTs enhances the ferroelectricity of PVDF.

Meanwhile, local piezoelectric hysteresis loops are measured by piezoresponse force microscope (PFM), in order to demonstrate the ferroelectricity increase in accordance with the β phase enhancement, as shown in Fig. 6. With the tip bias voltage sweeping, the composite curve shows obvious hysteresis loop, because of the vertical surface displacement movement, indicating the out-of-plane polarization in the composite film.35 On the other hand, the loop of the pristine PVDF shows scarce hysteresis, and the local phase responds to the applied tip bias immediately, indicating that the neat PVDF film has almost not ferroelectric nature.

Conclusions

PVDF/SWNT nanocomposites have been prepared by solution sonication method. The SWNTs were observed to form a well-dispersed random nanophase within the fluoropolymer matrix. The Raman spectra show that s-SWNTs are removed and only m-SWNTs are left in the composite. Furthermore, small-diameter m-SWNTs are preferable to interact with polymer due to Fermi electrons and enhanced curvature-induced strain. The selective dispersion of m-SWNTs helps the conversion of PVDF molecules from α-phase to β-phase during the crystallization of PVDF. The findings in our work are believed to be very significant for the fabrication and applications of PVDF nanocomposites.

Experimental section

Materials

PVDF powder (average molecular weight, M_w = 534,000, Sigma-Aldrich), HiPco SWNTs (1.1 nm in average diameter and 1.5 μm in average length, Unidym), and N,N-dimethylformamide solvent (DMF, 99.8%, Sigma-Aldrich) were used as received.

Preparation of PVDF/SWNT composite films

1 g of PVDF powder was dissolved in 25 ml of DMF solvent at 70℃ for 1 h to ensure complete dissolution, while 1 mg of SWNTs were dispersed in 25 ml of DMF solvent with tip-ultrasonic treatment at the power of 120 W for 1 h. Then, the SWNT suspensions were added drop wise to the PVDF solution with bath-ultrasonic treatment. The resultant mixture was centrifuged at 13,000 rpm for 30 min to remove the SWNTs bundles, and the supernatant was drop-cast on a glass dish and kept in oven at 110 ℃ for 15 min to ensure the removal of the solvent.

Characterization

Atomic force microscopy (AFM) image was obtained via a NanoScope IVA multimode atomic force microscope (DI Dimensions 3100) at tapping mode. The PVDF/SWNT composite films were prepared by drop-casting on a heavily-doped silicon substrate.

Raman spectra were recorded with a Renishaw InVia confocal micro Raman spectrometer using a 514.5 nm wavelength laser source. To avoid heating the sample, the laser power density was limited to 1 mW/μm^2.

Fourier transform infrared (FTIR) spectra were obtained using a Nicolet 6700 spectrometer in the range 400–4000 cm^{-1} to obtain the crystal structure for PVDF and nanocomposites.

Piezoresponse force microscopy (PFM) loops were obtained via a NanoScope IVA multimode atomic force microscope (DI Dimensions 3100) to demonstrate the ferroelectricity increase in PVDF/SWNT composite films.

Acknowledgements

This work was financially supported by the Special Funds for Major State Basic Research Projects of China (Grant No. 2011CBA00603), National Natural Science Foundation of China (Grant Nos. 61171010 and 61204090), Shanghai Municipal Natural Science Foundation (Grant No. 12ZR1402700), and Fundamental Research Project of young teachers to enhance research capacity of Fudan University (No. 20520133248).

Notes and references

State Key Lab of ASIC & System, School of Information Science and Technology, Fudan University, Shanghai, China. Fax: +86 21 55664269; E-mail: zjqiu@fudan.edu.cn (Z. J. Qiu), rliu@fudan.edu.cn (R. Liu)

1 S. Manna; A. Mandal and A. K. Nandi, *J. Phys. Chem. B*, 2010, **114**, 2342.
2 Z. -M. Dang, S. H. Yao and H. P. Xu, *Appl. Phys. Lett.*, 2007, **90**, 12907.
3 Y. Berdichevsky and Y.-H. Lo, *Adv. Mater.*, 2006, **18**, 122.
4 E. Peled, T. Duvdevani and A. Melman, *Electrochem. Solid-State Lett.*, 2000, **3**, 525.
5 X. Chen, X. Li, X. Qian, M. Lin, S. Wu, Q. Shen and Q. M. Zhang, *Polymer*, 2013, **54**, 5299.
6 X. Li, S. Lu, X. Chen, H. Gu, X. Qian and Q. M. Zhang, *J. Mater. Chem. C*, 2013, **1**, 23
7 N. Levi, R. Czerw, S. Xing, D. Iyer and D. L. Carroll, *Nano Lett.*, 2004, **4**, 1267.
8 S. Manna and A. K. Nandi, *J. Phys. Chem. C*, 2006, **110**, 14670.
9 C. A. Nguyen, S. G. Mhaisalkar, J. Ma and P.S. Lee, *Org. Electron.*, 2008, **9**, 1087.
10 J. P. Luongo, *J. Polym. Sci.*, 1972, **10**, 1119.
11 D. Yang, Y. J. Chen, *Mater. Sci. Lett.*, 1987, **6**, 599.
12 J. Scheinbeim, C. Nakafuku, B. A. Newman and K. D. Pae, *J. Appl. Phys.*, 1979, **50**, 4399.
13 Y. Konishi and M. Cakmak, *Polymer*, 2006, **47**, 5371.
14 H. P. Xu, Z. M. Dang, *Chem. Phys. Lett.*, 2007, **438**, 196.
15 G. X. Chen, Y. Li and H. Shimizu, *Carbon*, 2007, **45**, 2334.
16 P. Costa, J. Silva, V. Sencadas, C. M. Costa, F. W. J. van Hattum, J. G. Rocha, S. Lanceros-Mendez, *Carbon*, 2009, **47**, 2590.
17 Z. -M. Dang, L. Wang, Y. Yin, Q. Zhang and Q. -Q. Lei, *Adv. Mater.*, 2007, **19**, 852.

18 D. Chen, M. Wang, W. -D. Zhang and T. Liu, *J. Appl. Polym. Sci.*, 2009, **113**, 644.
19 Z. Zhao, W. Zheng, W. Yu and B. Long, *Carbon*, 2009, **47**, 2112.
20 X. Tang, M. Hou, L. Ge, J. Zou, R. Truss, W. Yang, M. Yang, Z. Zhu and R. Bao, *J. Appl. Polym. Sci.*, 2012, **125**, 592.
21 L. He, Q. Xu, C. Hua and R. Song, *Polym. Compos.*, 2010, **31**, 921.
22 R. Shvartzman-Cohen, E. Nativ-Roth, E. Baskaran, Y. Levi-Kalisman, I. Szleifer and R. Yerushalmi-Rozen, *J. Am. Chem. Soc.*, 2004, **126**, 14850.
23 L. He, J. Sun, X. Zheng, Q. Xu, R. Song, *J. Appl. Polym. Sci.*, 2011, **119**, 1905.
24 J. -K. Yuan, S. –H. Yao, Z. –M. Dang, A. Sylvestre, M. Genestoux and J. Bai, *J. Phys. Chem. C*, 2011, **115**, 5515.
25 H. Kataura, Y. Kumazawa, Y. Maniwa, I. Uemezu, S. Suzuki, Y. Ohtsuka and Y. Achiba, *Synth. Met.*, 1999, **103**, 2555.
26 S. M. Bachilo, M. S. Strano, C. Kittrell, R. H. Hauge, R. E. Smalley, R. B. Weisman, *Science*, 2002, **298**, 2361.
27 Z. Chen, W. Thiel, A. Hirsch, *Chem. Phys. Chem.*, 2003, **4**, 93.
28 A. Nish, J. -Y. Hwang, J. Doig and R. J. Nicholas, *Nature nanotechnology*, 2007, **2**, 640.
29 N. A. Rice, K. Soper, N. Zhou, E. Merschrod and Y. Zhao, *Chem. Commun.*, 2006, 4937.
30 S. D. M. Brown, A. Jorio, P. Corio, M. S. Dresselhaus, G. Dresselhaus, R. Saito and K. Kneipp, *Phys. Rev. B*, 2001, **63**, 155414.
31 R. Saito, T. Takeya, T. Kimura, G. Dresselhaus and M. S. Dresselhaus, *Phys. Rev. B*, 2001, **57**, 4145.
32 B. Mohammadi, A. A. Yousefi and S. M. Bellah, *Polym. Test.*, 2007, **26**, 42.
33 S. J. Doktycz and K. S. Suslick, *Science*, 1990, **247**, 1067.
34 A. Salimi and A. A. Yousefi, *Polym. Test.*, 2003, **22**, 699.
35 A. Gruverman and S. V. Kalinin, *J. Mater. Sci.*, 2006, **41**, 107.

+ PVDF

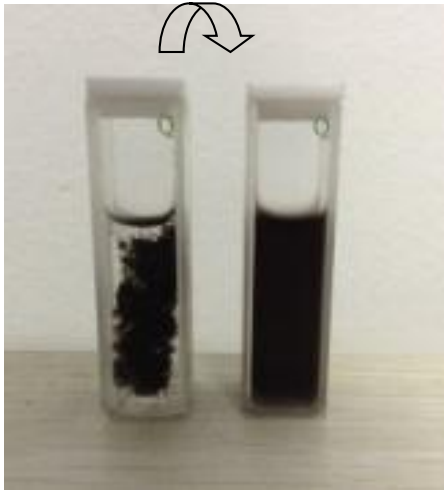

Raman spectra of RBM

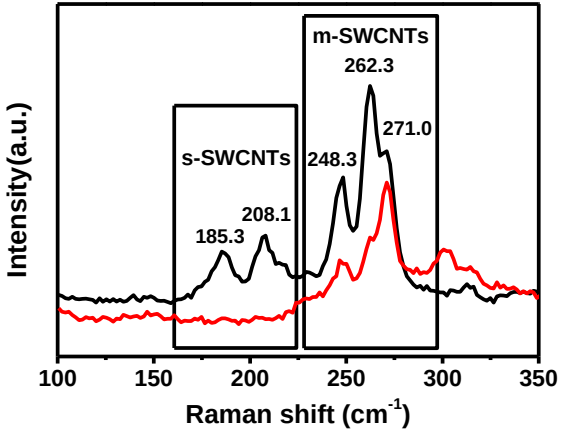

pristine SWNTs (black)
PVDF/SWNT composite (red)

FTIR spectra

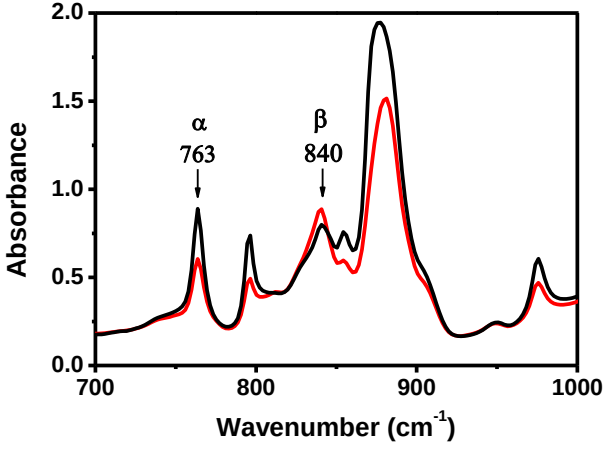

neat PVDF (black)
PVDF/SWNT composite (red)

Metallic-SWNTs of small diameters interact with PVDF more easily, and induce remarkable enhancement in the β ferroelectric phase of PVDF.